ORIGINAL ARTICLE

Experimental demonstration of 80 kW$_{th}$ chemical looping combustion of biogenic feedstock coupled with direct CO$_2$ utilization by exhaust gas methanation

Benjamin Fleiß[1] · Alexander Bartik[1] · Juraj Priscak[2] · Florian Benedikt[1] · Josef Fuchs[1] · Stefan Müller[1] · Hermann Hofbauer[1]

Abstract

Chemical looping combustion is a highly efficient CO$_2$ separation technology without direct contact between combustion air and fuel. A metal oxide is used as an oxygen carrier in dual fluidized beds to generate clean CO$_2$. The use of biomass is the focus of current research because of the possibility of negative CO$_2$ emissions and the utilization of biogenic carbon. The most commonly proposed OC are natural ores and residues, but complete combustion has not yet been achieved. In this work, the direct utilization of CLC exhaust gas for methane synthesis as an alternative route was investigated, where the gas components CO, CH$_4$ and H$_2$ are not disadvantageous but benefit the reactions in a methanation step. The whole process chain, the coupling of an 80 kW$_{th}$ pilot plant with gas cleaning and a 10 kW fluidized bed methanation unit were for this purpose established. As OC, ilmenite enhanced with limestone was used, combusting bark pellets in autothermal operation at over 1000 °C reaching high combustion efficiencies of up to 91.7%. The fuel reactor exhaust gas was mixed with hydrogen in the methanation reactor at 360 °C and converted with a methane yield of up to 97.3%. The study showed especially high carbon utilization efficiencies of 97% compared to competitor technologies. Based on the experimental results, a scale-up concept study showed the high potential of the combination of the technologies concerning the total efficiency and the adaptability to grid injection.

Keywords Chemical looping combustion · Methanation · CO$_2$ utilization · Pilot plant · Ilmenite · Biomass

1 Introduction

Chemical looping combustion (CLC) is an efficient carbon capture technology and utilizes the oxygen carrier capacity of certain metal oxides, called oxygen carrier (OC), to combust fuel to obtain undiluted CO$_2$ [4]. Through the use of the OC, there is no direct mixing of combustion air and fuel and therefore the exhaust gas is not diluted by nitrogen [5, 6]. Using biomass as fuel, CLC as a carbon capture and storage technology with bioenergy (BECCS) enables "negative" CO$_2$ emissions [7–10] or offers a resource for renewable and climate-neutral carbon [11]. Finding suitable OC is essential when converting solid fuels and compared to gaseous CLC, fuel impurities like ash pose additional challenges [12, 13]. Either cheap natural ores and residual materials, e.g., industrial waste, or highly specialized synthetic OC are used. [14, 15] The high cost of synthetic OC is critical due to the disadvantage of ash contamination leading to deactivation and dilution of the expensive OC during the process [15, 16]. Therefore, the general focus lies on natural ores and residual materials with the benefit of lower costs at the expense of reactivity and fuel conversion [17–19]. Mixing different ores, e.g., limestone addition to an OC, can improve conversion rates, but no full combustion with natural ores has been reported so far [20–24]. An extensive gas cleaning step is therefore essential for the successful utilization or storage of the biogenic CO$_2$ [25, 26]. An alternative route is the direct utilization of the CLC exhaust gas to produce, e.g., synthetic natural gas (SNG), where unburnt components like CO, CH$_4$ and H$_2$ are no burden but beneficial to the reactions in a methanation unit [27–29]. Other studies focus on different

✉ Benjamin Fleiß
benjamin.fleiss@tuwien.ac.at

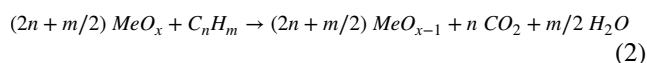[1] Institute of Chemical, Environmental and Bioscience Engineering, TU Wien, Vienna, Austria

[2] BEST – Bioenergy and Sustainable Technologies GmbH, Graz, Austria

utilization processes e.g., the production of ammonia or formic acid [30–33]. The combination of CLC and methanation has been covered so far only by different theoretical studies regarding economics and life cycle assessment [34–37]. This work shows the demonstration of the whole process chain in one lab facility. The exhaust gas of an 80 kW$_{th}$ CLC pilot plant, operated with ilmenite enhanced by limestone, is utilized in a fluidized bed methanation unit. Providing a proof of concept, this work deals with the following main objectives.

- First experimental demonstration of the coupled processes in a pilot scale; CLC combined with gas cleaning and direct methanation.
- Investigation of operation conditions, gas compositions, conversions and yields of the coupled processes.
- A scale-up concept study to a 100 MW$_{th}$ plant based on the experimental results, combining utilization and storage of biogenic CO$_2$.
- The scale-up simulation was in comparison to previous studies based on the experimental demonstration of the whole chain, incorporating impurities, gas cleaning steps and heat extraction [34–37].

2 Theory

CLC is an unmixed combustion technology where fuel and combustion air have no direct contact [5, 6]. Pure oxygen for fuel combustion is provided by a metal oxide (MeO_x) called the oxygen carrier (OC) in form of lattice oxygen. The OC enters two different reaction zones located in two reactors, according to Fig. 1. In the air reactor (AR), the OC takes up oxygen during a reaction with air (Reaction 1). The combustion of the fuel occurs in the fuel reactor (FR), where the transfer of oxygen to the fuel (C_nH_m) is enabled, as seen in Reaction 2. [38] Thereby the OC is reduced and oxidation is again necessary for completing the loop of the two reactions. Due to the absence of nitrogen, the exhaust gas of the FR consists of CO$_2$ and H$_2$O. The circulation of OC between the reactors transfers the oxygen necessary for combustion and the heat required to maintain the heat balance in the system [39].

$$MeO_{x-1} + 1/2 O_2 \rightarrow MeO_x \tag{1}$$

$$(2n + m/2) \, MeO_x + C_nH_m \rightarrow (2n + m/2) \, MeO_{x-1} + n \, CO_2 + m/2 \, H_2O \tag{2}$$

The OC must fulfill several requirements to be suitable for CLC operation. A sufficient oxygen transport capacity with high reactivity for reduction and oxidation reactions maintained over a large number of redox cycles is essential. Good fluidization properties, resistance to agglomeration and attrition are also fundamental for a stable operation [40].

Elutriated fines and dilution with ash increase the replacement costs of OC. Therefore, economical oxygen carriers with enough oxygen transport capacity, such as iron or manganese ores, and iron-containing wastes have mainly been proposed for the combustion of solid fuel in CLC [14]. Mentioned materials show no or no permanent capabilities of the chemical looping with oxygen uncoupling (CLOU) effect, which is needed for complete solid fuel combustion [41]. Therefore, an extensive gas cleaning step is essential for successful utilization or storage applications. The largest cost factor of solid CLC is therefore the complete conversion of unburnt gases in an oxy-polishing process, where pure oxygen is needed [25].

As an alternative, subsequent methanation of the exhaust gas of CLC is proposed in this work to reduce gas treatment costs and produce biogenic methane as a product. For this process, additional external H$_2$ is needed. During catalytic methanation, H$_2$ and CO react to CH$_4$ and H$_2$O according to Reaction 3. The reversed water–gas shift reaction (Reaction 4) leads to the formation of CO and H$_2$O if excessive hydrogen is available. In combination with Reaction 3, CO$_2$ and H$_2$ react via the reversed water–gas shift reaction and form CH$_4$ and H$_2$O, as seen in Reaction 5.
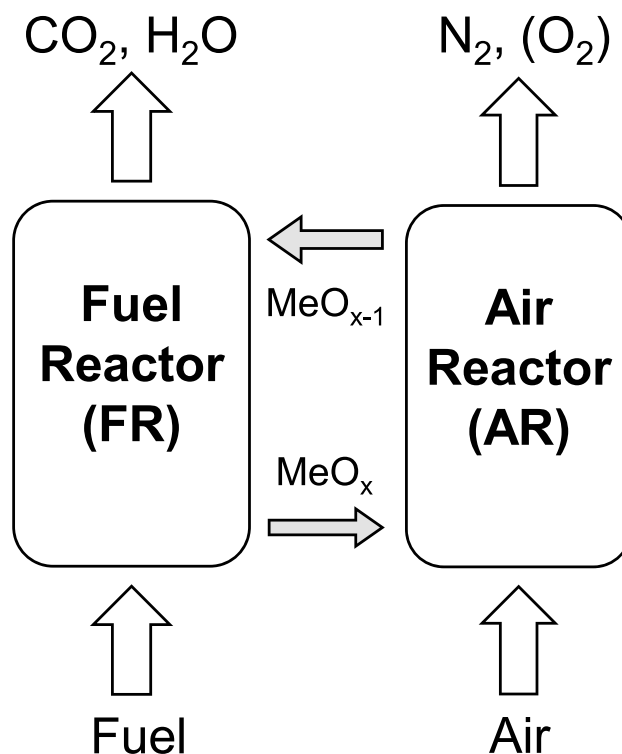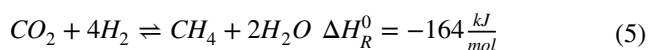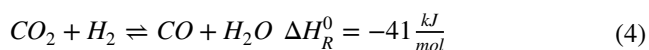
$$CO + 3H_2 \rightleftharpoons CH_4 + H_2O \quad \Delta H_R^0 = -206 \tfrac{kJ}{mol} \tag{3}$$

Fig. 1 Scheme of the CLC process with AR and FR

$$CO_2 + H_2 \rightleftharpoons CO + H_2O \quad \Delta H_R^0 = -41 \frac{kJ}{mol} \qquad (4)$$

$$CO_2 + 4H_2 \rightleftharpoons CH_4 + 2H_2O \quad \Delta H_R^0 = -164 \frac{kJ}{mol} \qquad (5)$$

All these reactions are exothermic, and large quantities of heat need to be removed. For this case, fluidized beds possess high heat and mass transfer capabilities due to the movement of the particles and therefore can tackle this issue [42].

3 Materials and Methods

3.1 Process chain setup

For the utilization of the FR exhaust gas, a complete process chain has been set up at TU Wien, consisting of the advanced dual fluidized bed (DFB) reactor, a gas cleaning section and a fluidized bed methanation reactor. Figure 2 depicts the process chain of the investigated FR exhaust gas treatment route, including the methanation unit at TU Wien. A partial flow of the exhaust gas from the fuel reactor of the CLC pilot plant enters the gas cleaning section and is subsequently catalytically converted to raw-SNG in the methanation reactor with externally supplied hydrogen.

The 80 kW$_{th}$ CLC pilot plant at TU Wien has been proposed as an advanced DFB system by Pröll and Hofbauer [43] for solid fuel CLC and Schmid et al. [44] for fluidized bed steam gasification, also seen in Fig. 3. The two fluidized beds (AR and FR) are connected at the top and bottom via steam-fluidized loop seals. These loop seals separate the gas atmospheres between the reactors to ensure CO_2 purity and high capture rates of carbon. The AR works as a riser to initiate the circulation of the bed material between the reactors. Air staging in the AR enables control over the amount of OC transported up the riser. The entrained particles from the AR are separated by a gravity separator and transported to the FR via the upper loop seal (ULS). The upper part of the FR is a counter-current column with several built-in constrictions placed along its height. They reduce the free cross-section of the reactor to intensify the gas–solid contact by increasing the solid hold-up of the downward-flowing OC. In contrast, the lower part of the FR is designed as a bubbling fluidized bed to reach a high solid residence time. The FR is operated with steam acting as a fluidization and gasification agent for solid fuels. The loop of bed material is closed by the lower loop seal (LLS), where the OC is transported back to the AR. The fuel feed is realized in the lower part of the FR by a screw conveyer with on-bed feeding. To compensate for heat losses over the reactor wall, it is possible to introduce auxiliary fuel in the form of heating oil to the AR. More detailed reactor and cold flow model descriptions are found in the literature [1, 45, 46].

Because of the different scales of the gas cleaning units and the methanation unit compared with the CLC reactor, only a partial flow of the exhaust gas from the FR is redirected to the utilization route. The gas cleaning section consists of a particle filter, a biodiesel scrubber and adsorptive beds for the removal of impurities. Heavy tars and water-soluble substances are removed in the biodiesel scrubber while light tars and sulfur compounds are held back in activated carbon filters and a ZnO guard bed. The methanation reaction itself takes place in a single-step fluidized bed reactor (cf. Figure 4) at ambient pressure and temperatures around 360 °C. The necessary hydrogen was provided by a gas bottle. Multiple temperature measurements together with the air cooling allow an isothermal operation of the fluidized bed methanation reactor. The reactor is designed for a nominal raw-SNG output of 10 kW and utilizes 1.5 kg of a specially prepared, attrition-resistant NiO/Al$_2$O$_3$ catalyst for fluidized bed applications. The catalyst for the methanation contained 20 wt.-% NiO and 2 wt.-% MgO and was prepared on an Al$_2$O$_3$ support. The used support was a Puralox SCCa-150/200 -Al$_2$O$_3$ from SASOL, which is particularly designed for fluidized bed applications and thus exhibits a high level of attrition resistance. Additional information on the catalyst is published by Bartik et al. [47]. A detailed description of the process chain, the reactor setup and the gas cleaning route is reported elsewhere [42, 47].
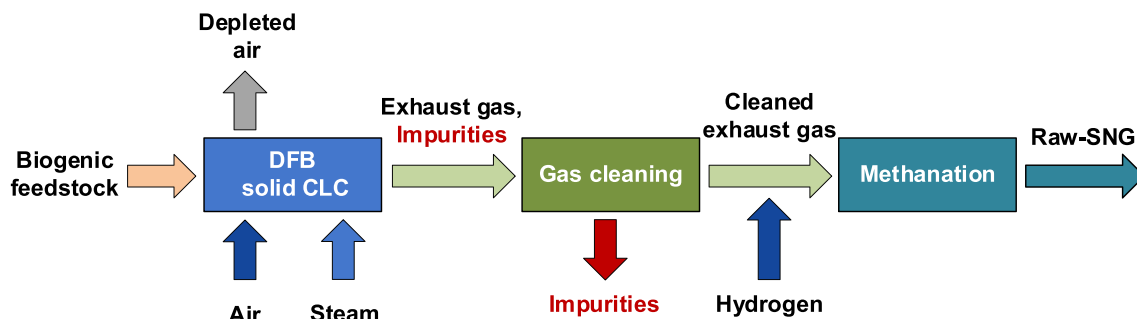

Fig. 2 Process chain of the direct utilization of chemical looping combustion exhaust gas to raw-SNG
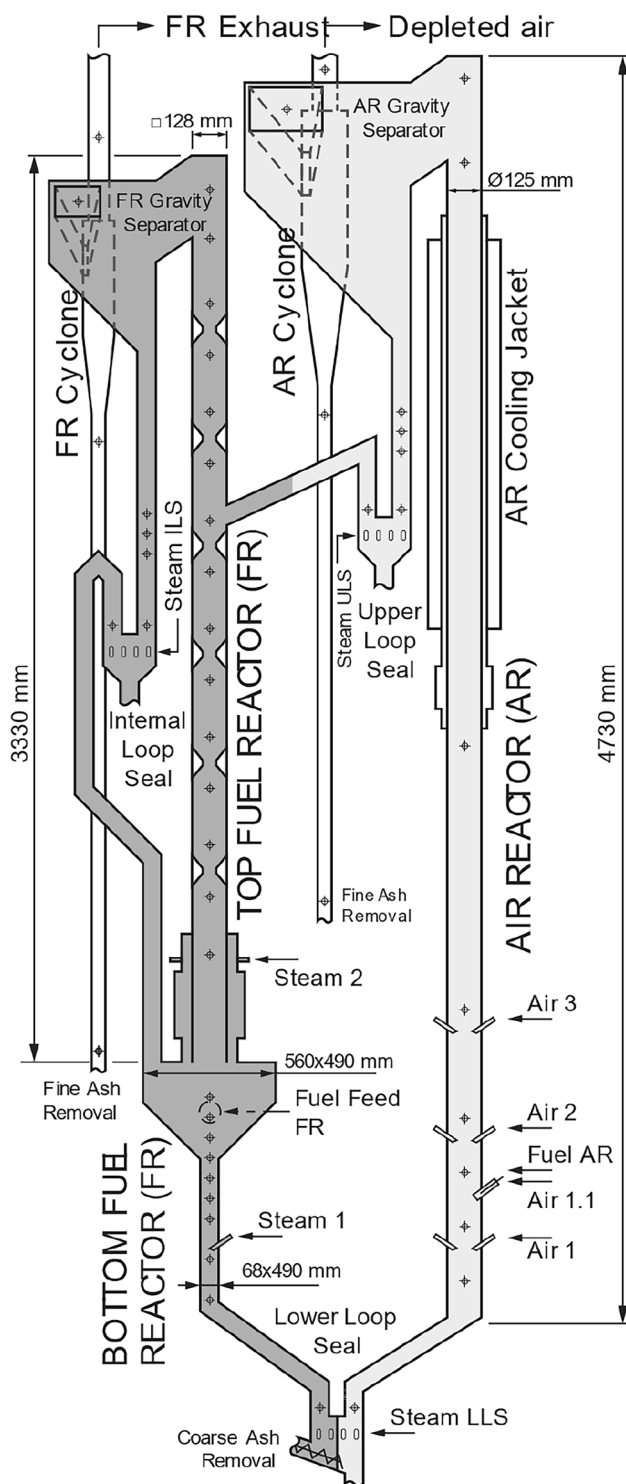
Fig. 3 Scheme of the 80 kW$_{th}$ pilot plant at TU Wien, divided into FR on the left and AR on the right side, adapted from [1]

3.2 Material characterization

Ilmenite, a natural iron titanium ore, mixed with 20 wt% of limestone was used as OC for this experiment. Ilmenite

can still be considered as the best-investigated benchmark material for solid fuel CLC [48–54]. It is a so-called heterogeneous OC, i.e., it is not able to release gaseous oxygen and the fuel conversion happens solely via gas–solid contact [48]. The limestone was purchased as feed limestone. The $CaCO_3$ of the limestone reacts to CaO under the conditions in the reactor system and, thus, releases CO_2 in the reactor while heating up. Limestone addition is known for improving gas conversion, because of the catalytic effect of CaO on the water–gas shift reaction, converting CO to CO_2 [55]. Also, limestone binds parts of the fuel sulphur and improves the exhaust gas quality [52, 56]. The compositions of both materials can be found in Table 1.

The characterization of the OC, according to Fleiß et al. [3], provides an estimation of the impact of blending ilmenite with limestone on different important parameters, conducted in a laboratory facility [57]. Visualization in a spider-chart depicts the suitable properties as a material for fluidized beds on the right side and the oxygen carrier-specific properties on the left side, as seen in Fig. 5, regarding being a suitable OC. By blending ilmenite with limestone, the properties listed on the left side of the diagram could be improved. Thereby, oxygen carrier-specific properties like oxygen transport, gas conversion and carbon conversion show higher numbers due to an increased reactivity and catalytic effect with limestone at the expense of bed material properties. The highest decrease is shown in the attrition resistance resulting from the porous structure of limestone. By shifting the area to the middle of the chart, limestone addition has a high potential for the 80 kW$_{th}$ pilot plant.

The used fuel was bark pellets made from commercially available bark mulch. It was first milled and then processed in the pelletizing machine with the addition of a small amount of water. After drying, the resulting pellets had a diameter of about 6 mm and a length of 5–25 mm. The fuel analysis of the bark pellets is shown in Table 2.

3.3 Experimental evaluation and performance indicator

A detailed description of the experimental setup and procedure is given by Penthor et al. [1] and by Fleiß et al. [3, 58]. The goal of each operating point is to achieve stable operations with the highest possible conversion to CO_2. To have a clear overview of the experimental conditions, there are several temperature and pressure measurements spread over both reactors. In addition, the components of the gases after FR, AR and methanation unit are measured by Rosemount NGA 2000 gas analyzers (used methods: UV/IF, paramagnetic and heat conductivity), which have accuracy at about 1% of their measuring range. In the AR exhaust gas CO_2, CO and O_2 are measured. In the FR exhaust gas, a gas chromatographic measurement is carried out in addition to a continuous

Fig. 4 3D-CAD drawing (left) and picture (right) of the fluidized bed reactor [47]
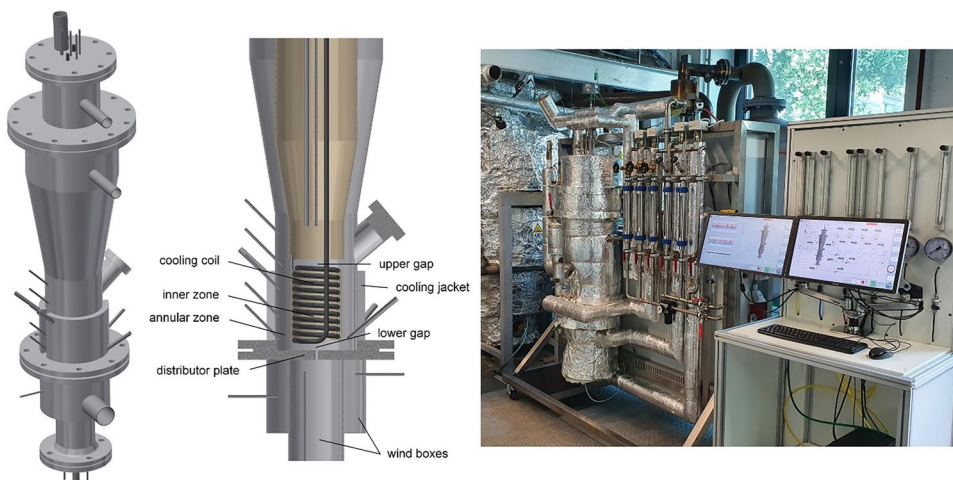
measurement of the concentration of gases. The gas components measured include O_2, CO_2, CO, CH_4, H_2, N_2, C_2H_2, C_2H_4 and C_2H_6. Based on the available measurements and the known input flows, a complete mass and energy balance could be calculated for each steady-state experimental point of the CLC part via the simulation software IPSEpro [58, 59]. In the validation mode of the software, a standard accuracy of 10%, except for temperature measurements (10 °C), was selected for every single measurement calculating also the relative sum of square errors, seen in Table S1 of the supplementary material. The most likely experimental conditions were calculated with a confidence interval of 95%, while still fulfilling all mass and energy balances. By balancing input and output measurement, the calculation validates each measurement by its accuracy in comparison to the overdetermined system. To evaluate and assess the performance of the OC and the operating point in

the plant, important key performance indicators (KPIs) can be determined. The following paragraphs feature important KPIs for the CLC section of the experiments. One important KPI, the carbon capture rate η_{CC} describes how much of the carbon introduced into the fuel reactor is found in the gas phase of the fuel reactor exhaust gas. This also represents the loss of carbon, mainly through combustion in the air reactor.

$$\eta_{CC} = \frac{\dot{n}_{C,FR,exhaust}}{\dot{n}_{C,FR,feed}} \cdot 100[\%] \qquad (6)$$

The CO_2 yield γ_{CO2} describes how much of the carbon introduced into the fuel reactor is contained in the fuel reactor exhaust gas as CO_2. It is a measure of the incomplete conversion of carbon to CO_2.

$$\gamma_{CO_2} = \frac{\dot{n}_{CO_2,FR,exhaust}}{\dot{n}_{C,FR,feed}} \cdot 100[\%] \qquad (7)$$

Table 1 Composition of the Norwegian ilmenite and calcined limestone (components ≥ 0.1 wt%)

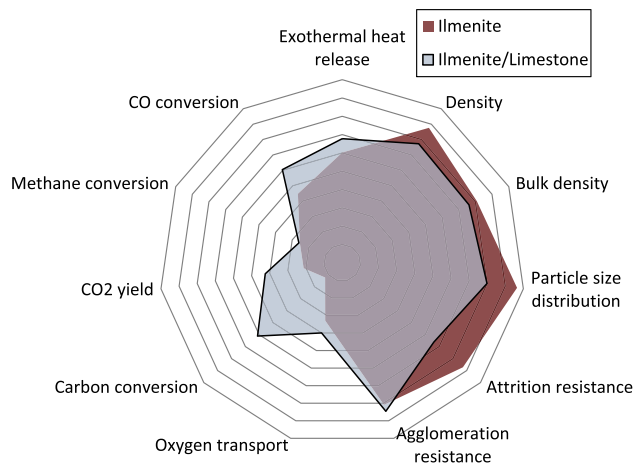| Content [wt%]	Ilmenite	Calcined limestone
TiO_2	44.1	-
Fe^{2+}	25.9	0.1
Fe^{3+}	9.1	-
O with Fe	11.4	0.1
MgO	3.6	4.4
SiO_2	2.0	0.8
Na_2O	-	4.2
MnO	0.3	-
CaO	0.3	88.4
V_2O_3	0.2	-
S	0.1	0.1
Cr_2O_3	0.1	-
Al_2O_3	0.6	0.8
Cl	-	0.8

Fig. 5 Characterization and comparison of the mixture of ilmenite and limestone to pure ilmenite as OC (adapted from [3])

Table 2 Fuel analysis of the bark pellets

Component	Content	Parameter	Value
Carbon (C)	47.1 wt%(wf)	Water content	5.3 wt%
Hydrogen (H)	5.1 wt%(wf)	Volatile content	70.5 wt%(waf)
Nitrogen (N)	0.6 wt%(wf)	Fixed carbon	29.5 wt%(waf)
Sulphur (S)	0.05 wt%(wf)	LHV (dry)	16.9 MJ/kg(wf)
Chlorine (Cl)	<0.01 wt%(wf)	LHV (moist)	15.9 MJ/kg
Oxygen (O)	35.7 wt%(wf)	Ash	11.46 wt%(wf)

The CO_2 selectivity S_{CO2} is a measure whether the combustion of the carbon $\dot{n}_{C,FR,exhaust}$ in the exhaust gas to CO_2 is complete, see Eq. 8. The difference of S_{CO2} to 100% represents the amount of unburnt carbon in the FR exhaust gas in components like CO, CH_4, higher hydrocarbons and tars.

$$S_{CO_2} = \frac{\dot{n}_{CO_2,FR,exhaust}}{\dot{n}_{C,FR,exhaust}} \cdot 100[\%] \tag{8}$$

Another important KPI is the combustion efficiency η_{Comb} describing how much of the fuel is converted to CO_2 and H_2O. It combines the unconverted gases with the lost fuel to the AR reactor and gives an overall assessment of the CLC operation, shown in Eq. 9. It is based on the ratio of the demanded oxygen for complete stoichiometric combustion of the exhaust gas $\dot{n}_{O_2,exhaust,dem}$ and of the fuel $\dot{n}_{O_2,fuel,dem}$.

$$\eta_{Comb} = \left(1 - \frac{\dot{n}_{O_2,exhaust,dem}}{\dot{n}_{O_2,fuel,dem}}\right) \cdot 100[\%] \tag{9}$$

The total oxygen demand Ω_{OD} describes the amount of oxygen necessary for the complete oxidation of the FR exhaust gas compared to the amount of oxygen necessary for full the oxidation of the fuel feed, see Eq. 10.

$$\Omega_{OD} = \frac{\dot{n}_{O_2,exhaust,dem}}{\dot{n}_{O_2,fuel,dem}} \cdot 100[\%] \tag{10}$$

Important KPIs concerning the methanation section are displayed in Eq. 11–14. The methane yield (Y_{CH_4}) is calculated according to Eq. 10, where $\dot{n}$ is the molar flow and N is the number of carbon atoms in the respective gas component in the feed gas (*feed*) and the raw-SNG (*out*). Equation 12–14 define the CO conversion (X_{CO}), the CO_2 conversion (X_{CO_2}) and the H_2 conversion (X_{H_2}), respectively.

$$Y_{SNG,CH_4} = \frac{\dot{n}_{CH_4,out}}{\sum_i N_i \dot{n}_{i,feed}} \cdot 100[\%] \tag{11}$$

$$X_{SNG,CO_2} = \frac{\dot{n}_{CO_2,feed} - \dot{n}_{CO_2,out}}{\dot{n}_{CO_2,feed}} \cdot 100[\%] \tag{12}$$

$$X_{SNG,CO} = \frac{\dot{n}_{CO,feed} - \dot{n}_{CO,out}}{\dot{n}_{CO,feed}} \cdot 100[\%] \tag{13}$$

$$X_{SNG,H_2} = \frac{\dot{n}_{H_2,feed} - \dot{n}_{H_2,out}}{\dot{n}_{H_2,feed}} * 100[\%] \tag{14}$$

The stoichiometric number (*SN*) (Eq. 15) evaluates the product gas in terms of its stoichiometry for methanation. The amount of hydrogen content is put in relation to the content of carbonaceous species to be methanated according to the corresponding reaction equations.

$$SN = \frac{y_{H_2}}{3\,y_{CO} + 4\,y_{CO_2}}[-] \tag{15}$$

The overall process chain is evaluated through the overall cold gas efficiency (CGE) according to Eq. 16. It relates the chemical energy of methane in the raw-SNG to the chemical energy of the fuel input to the FR plus the chemical energy introduced through the external hydrogen addition. The chemical energy is based on the lower heating value.

$$CGE = \frac{P_{CH4,out}}{P_{fuel,FR} + P_{H_2}} * 100[\%] \tag{16}$$

Equation 17 shows the carbon utilization efficiency ($\eta_{C,total}$) of the whole experimental chain, which assesses the amount of carbon in the CH_4 of the raw-SNG compared to the amount of carbon introduced via the fuel in the FR.

$$\eta_{C,total} = \frac{\dot{n}_{C,CH_4,out}}{\dot{n}_{C,FR,feed}} * 100[\%] \tag{17}$$

4 Results and Discussion

4.1 General operation

The start-up procedure of the pilot plant was divided into two different phases. During the first phase, the pilot plant was preheated by the fluidization of the AR and FR (air for both reactors) up to 350 to 400 °C using electrical heating. When the plant temperature was high enough, light fuel oil (AR) and wood pellets (FR) were fed into the plant. At 900° C, the air supply to the FR was gradually replaced by steam to initiate CLC operation. After the ramp-up of the temperatures and the change of fuel from wood pellets to bark pellets, the continuous operation started at 18:00, see Fig. 6. The green areas mark steady-state operating conditions with only minor changes in temperatures, concentrations and material transport. During operating point 1 (OP1),

high temperatures were reached ensured by oil addition. CO_2 concentrations up to 88% were achieved, whereby a few percent of nitrogen diluted the FR exhaust gas through the flushing of the fuel bunker and the pressure cells. During operating point 2, no oil was added and thus the temperature in both reactors decreased while higher CO_2 concentrations were reached. Because of the autothermal operation, OP2 was also characterized by lower temperature fluctuations in the AR. The temperature of the AR was kept at a high level through the exothermal oxidation reaction of the OC, while the temperature of the FR showed a slight decrease over time. At 18:00, the methanation unit was activated. The high peaks of the H_2 concentration or the grey marked areas are a result of changing the operation condition of the methanation unit. With excess hydrogen, it was possible to convert almost all CO_2 to methane. During OP2b the excess hydrogen was increased to minimize the CO_2 and CO in the raw-SNG. Overall, the operation of both reactors was highly stable and no interference, e.g., defluidization or agglomeration occurred. The grey areas in Fig. 6 do not show an impairment of operation, but a short interruption of the gas measurement.

## 4.2 Comparison of autothermal CLC operation (OP2) and CLC with oil addition (OP1)

During the two operating points OP1 (with oil addition) and OP2 (autothermal), the input parameters were not changed for the whole duration, resulting in only minimal changes in reactor temperatures and gas concentration. At the start of OP2, the oil addition to the AR was stopped and autothermal conditions were reached. That means that besides the addition of bark pellets to the FR and gas preheating, no additional heating of the FR took place. Of all values, the

temperature in the FR changed the most during OP2. The high heat losses through the reactor wall and the autothermal operation caused a slight drop in temperature, which slowly levelled off because of the heat losses and the generated heat balanced out. The concentration of the gases in the FR was not impacted by the slight temperature drop during OP2.

Figure 7 presents the average temperature profiles over the AR and FR for both operating points. In general, 10 to 20 °C higher temperatures were achieved at OP1, but the most significant temperature difference was measured in the AR at 1.5 m height. The temperature elevation resulted from the oil injection and the heat release due to oil combustion. In the temperature profile of the FR, the energy demand for the degasification of the fuel is visible. In the bubbling bed of the FR, the temperature dropped over 100 °C. High temperatures in this part of the reactor are essential to favor gasification kinetics and therefore minimize carbon losses to the AR. In the upper part of the FR, the temperature increased due to the combustion of the unburnt gases and the inlet of hot OC coming from the AR. In this part, the temperature difference of the operating points dwindled because of a higher gas conversion of OP2. In large-scale reactors, relative heat losses would be considerably lower due to the better insulation and refractory lining, which is not available in the 80 kW$_{th}$ pilot plant. In addition, the scale-up of fluidized beds is beneficial for the specific surface of the plant, which also reduces heat losses and the temperature of the AR would be adjustable by a reactor wall cooling [60].

The decrease of the FR temperature resulted also from the change of the solid circulation rate of hot OC between OP1 and OP2, which was a result of the lower airflow of OP2. In autothermal operation, no air is needed for oil combustion and the excess air was reduced to reach similar oxygen concentrations of the AR exhaust gas. The higher

Fig. 6 Gas concentration in the FR and temperatures of the FR and AR (left). Raw-SNG gas concentrations downstream the methanation unit (right)
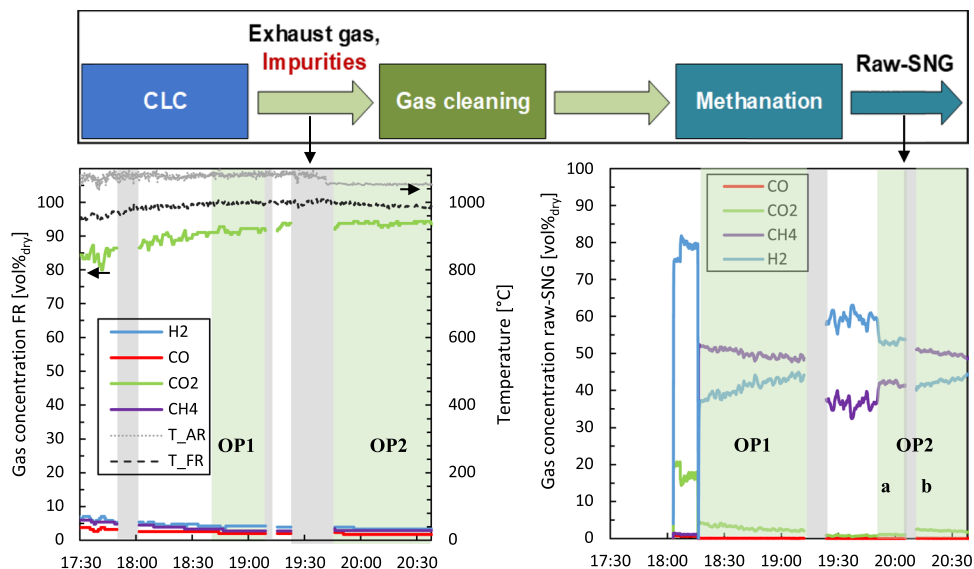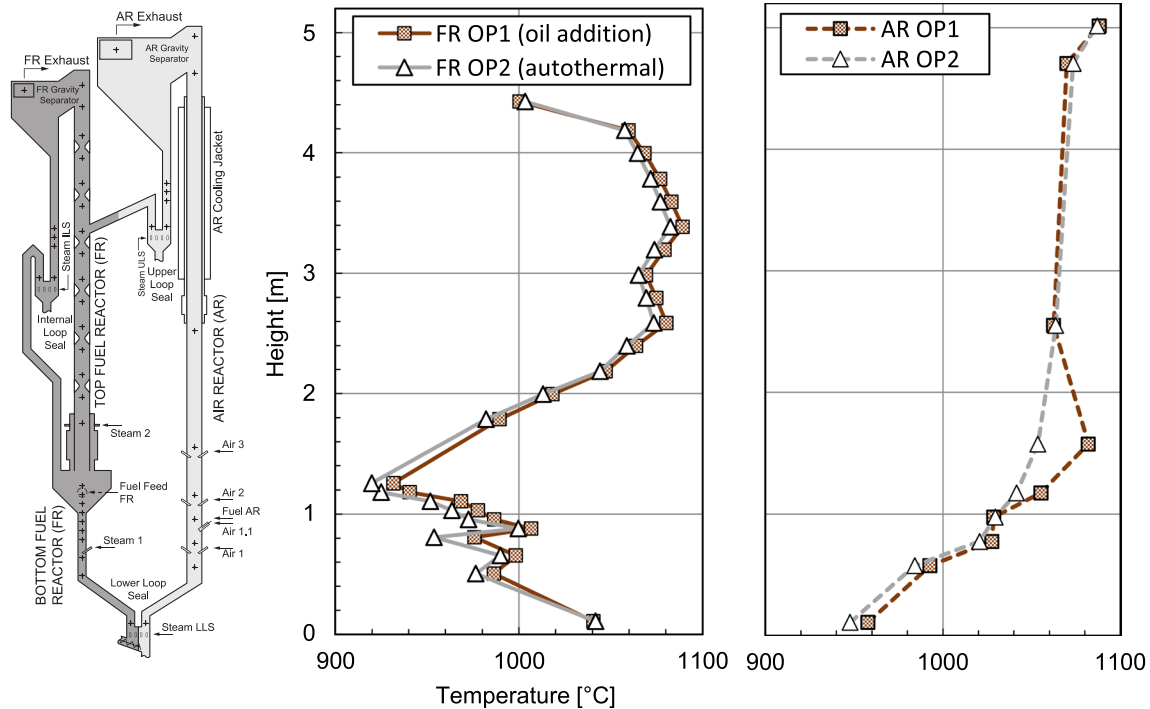
Fig. 7 Temperature profile over both reactors, FR and AR, of OP1 with oil addition as well as the autothermal OP2

solid circulation of OC led to more heat transport to the FR. The increased solid circulation rate, see Table 3, led to additional hot OC in the lower FR and therefore to higher temperatures, which benefited the gasification reaction of char resulting in higher carbon capture rates. The carbon capture rate was determined by the measurement of a CO_2 concentration of the AR exhaust gas to evaluate the slip of char from the FR. Due to the oil injection in OP1 the CO_2 concentration of the AR exhaust gas was higher than in the other experiments. The carbon injected by oil is not included in the carbon capture rate balance, because the oil should compensate for heat loss over the reactor wall, which would be reduced in industrial reactors. The additional input of carbon by oil decreases the accuracy of the carbon capture rate value. The calculation is only based on the CO_2 measurement in the AR and seems therefore not completely reliable, because of the high uncertainty of the oil and bark

fuel input. This is also shown by the higher deviation of the validation calculation compared to other measurements at 5–15%, seen in Table S1 of the supplementary material. In contrast to the results in Table 3, higher solid circulation rates usually decrease the carbon capture rate, according to the previous experiments [58].

Although no higher hydrocarbons were measured by gas chromatography in both operating points, Fig. 8 shows that the fuel conversion was not complete. Concentrations of unconverted CH_4, CO and H_2 and low amounts of tars in the FR exhaust gas were measured, which are similar or lower according to the literature [56, 61]. Tars were measured according to the measuring method of Benedikt et al. [2]. Comparing the operating points, OP2 showed lower gas concentrations of CO and H_2 as well as a lower tar content in the FR exhaust gas. The higher temperature of OP1 benefited the decomposition of CH_4 into smaller

Table 3 Air fluidizing and staging of the AR resulting in different solid circulation rates

	OC to fuel ratio	AR air input total	Primary	Secondary	Tertiary	Oil air	Solid Circulation rate	Carbon capture rate
	[-]	[Nm³/h]	[Nm³/h]	[Nm³/h]	[Nm³/h]	[Nm³/h]	[kg/h]	[-]
OP1 (Oil addition)	3.0	94.9	31.5	40.8	17.6	5.0	1503.6	99.5
OP2 (autothermal)	2.7	72.5	17.4	30.1	19.9	5.1	1138.1	95.8

gas components. The advantage of higher temperatures with oil addition to the AR seemed to enhance operation partly regarding to carbon capture rate and methane conversion. In return, the oxidation of the ilmenite in the AR was hindered by the oxygen consumption of oil and affected the gas conversion in the FR adversely. The reason could be attributed to a lower oxidation state of OC in the AR during OP1 due to the oil injection despite higher air flows. Oil addition is a viable tool for heating up the pilot plant or reaching plateaus of high temperature, but interfered too much with stationary CLC operation and is in the case of CLC not suitable to simulate the operation of industrial plants. For the energy production in scale-up plants, extraction of heat over the AR reactor wall could be possible, which is comparable to the heat loss of the pilot plant. An experimental simulation of scale-up operation is therefore better matched with autothermal conditions in the pilot plant. The major difference is the adjustable temperature in the AR over the heat extraction, which in the case of the pilot plant is not given. Steady-state operation in the pilot plant is therefore more limited to certain process condition. The temperature of the system is not directly controllable but is a result of different parameters, e.g., solid circulation, fuel addition in the FR and airflow in the AR. In this respect, a more in-depth interpretation of the operation than here would require considerably more different experimental points and thus more operating time.
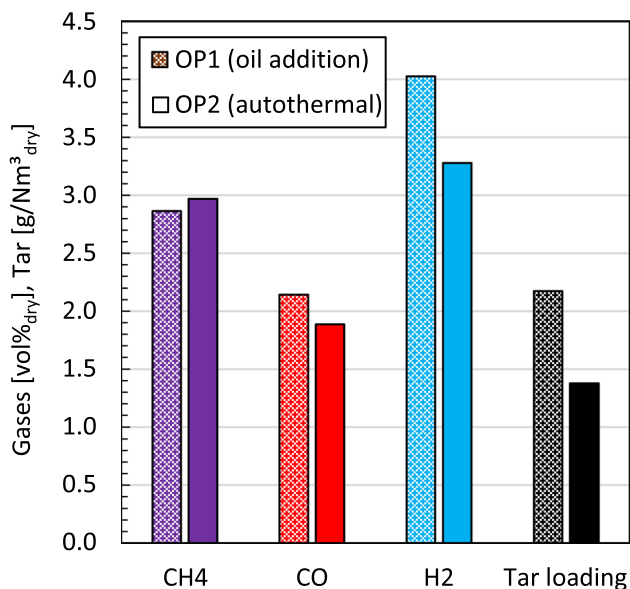

Fig. 8 Unconverted species of the FR exhaust gas OP1 with oil addition in comparison to autothermal OP2. Tars were measured according to Benedikt et al. [2] and included GC/MS with BETX but without toluene

4.3 Comparison of pure ilmenite with ilmenite and limestone addition

Recent experiments on the pilot plant were conducted with four different OC and five different fuels, published by Fleiß et al. [58]. For comparison, the results of pure ilmenite and pelletized bark were of interest. Table 4 shows the important parameters and results of experiments with both pure ilmenite and the mixture of ilmenite with limestone. With pure ilmenite, higher solid circulation rates were reached due to the lower density of limestone, resulting in a higher OC-to-fuel ratio despite higher fuel input. The main difference was the higher temperature reached during the experiments with limestone addition. In the experiments with pure ilmenite, the temperature was ramped up with oil to over 1000 °C but was levelling off to lower temperatures without additional heating. Due to lower conversion rates of unburnt gases like CO, CH_4 and H_2, the energy demand of the FR was higher due to less heat release because of the incomplete combustion and higher energy demand of the gasification reaction. The lower temperatures with pure ilmenite also led to a higher loading of tar at around 13.4 g/Nm^3_{dry} (compare Fig. 8) and the formation of higher hydrocarbons. The catalytic effect of limestone regarding the reduction of tars is known in literature [52]. The carbon capture rate was also higher in the experiments with limestone addition. The experiments with limestone addition showed not only a higher performance regarding carbon capture rate but especially combustion efficiency, CO_2 yield and selectivity reached higher numbers, see Fig. 9. The operating conditions of the different experiments indicate why the performance of OP1 and OP2 turned out to be higher. On the one hand, the power input to the FR was lower during the experiments with limestone. A higher solid circulation rate was thus necessary to transport sufficient heat and oxygen with pure ilmenite, which can reduce the carbon capture rate [58]. The FR was operated with steam and through the increased fuel input, a lower steam-to-carbon ratio resulted in disadvantageous conditions for the gasification reaction of fuel with pure ilmenite [62]. On the other hand, there was a temperature gap of 100 to 150 °C between the experiments with and without the addition of limestone. The high temperatures in the case of the ilmenite/limestone mixture, especially in the autothermal operation of OP2, had a major impact on the conversion of tar and gases in the FR reactor and resulted in higher combustion efficiency. The catalytic effect initiated by limestone benefited the water–gas shift reaction reducing the CO and increasing the H_2 concentration, which is more reactive with ilmenite [52, 56]. The additional heat released due to the higher conversion rates of gas resulted in higher temperatures in the FR, which favoured the oxygen release of the OC and again benefited thereby the gas conversion. Although the total oxygen transport capacity of ilmenite

Table 4 Results of the experimental campaigns on the 80 kW pilot plant, comparison of results of ilmenite and ilmenite mixed with limestone

Name	Symbol	Unit	Bark_1.1	Bark_1.2	OP1 (Oil AR)	OP2 (autothermal)	Typical reactor values
Source	-	-	[58]	[58]	this study	this study	[1, 3, 58]
Fuel	-	-	Bark	Bark	Bark	Bark	Various
Bed material	OC	-	Ilmenite	Ilmenite	Ilmenite/ Limestone	Ilmenite/ Limestone	Natural ores
Fuel power input FR	$P_{fuel,FR}$	[kW]	77.7	78.2	71.8	62.0	50–85
Fuel power oil to AR	P_{oil}	[kW]	0	0	17.6	0	0–20
Solid circulation rate	SCR	[kg/h]	1726	1734	1504	1138	1000–2000
OC to fuel ratio	φ	[-]	3.2	3.2	3	2.7	2–6
S/C ratio	S/C	[-]	1.1	0.8	1.4	1.5	1–2.5
Air-to-fuel ratio	λ	[-]	1.3	1.2	1.5	1.3	1.2–1.8
Temperature gas AR	ϑAR_{exh}	[°C]	916	914	1026	1028	900–1000
Temperature gas FR	ϑFR_{exh}	[°C]	920	913	1056	1054	900–1000
Lower FR	ϑFR_{low}	[°C]	876	869	986	976	850–950
O_2 demand	Ω_{OD}	[%]	18.1	17.4	9	8.4	10–30
Carbon capture rate	η_{CC}	[%]	94.9	95.2	99.5	95.8	90–98
Combustion efficiency	η_{comb}	[%]	81.9	82.6	91	91.7	70–90
CO_2 yield	γ_{CO2}	[%]	82.9	85.4	93.3	90.3	70–90
CO_2 selectivity	S_{CO2}	[%]	87.4	89.8	94.7	94.9	75–90

mixed with limestone is lower, it was capable of releasing more oxygen. With given performance parameters, not only the previous experiments with bark were surpassed, but also the highest combustion efficiency, CO_2 yield and selectivity were achieved in this reactor setup with natural ores so far [1, 58]. The gas conversion, similar to the CO_2 selectivity, generally decreases with the concentration of volatiles in the fuel. However, to reach high selectivities up to 95% with a high volatile fuel like bark is usually only reached with OC capable of the CLOU effect, e.g., copper ore, manganese ore

or synthetic OC [63]. This highlights both the importance of blending natural ores for boosting the reactivity, but also the proper reactor setup in combination with OC and operation conditions, especially high temperatures for the conversion of different gas species. The OC must maintain stability and agglomeration resistance at high temperatures, which was the case for the ilmenite/limestone blend. Nevertheless, complete combustion of fuel has not been reached with currently available natural ores or residue materials yet. For this reason, a concept for further treatment of the exhaust gas must be available for commercial plants.
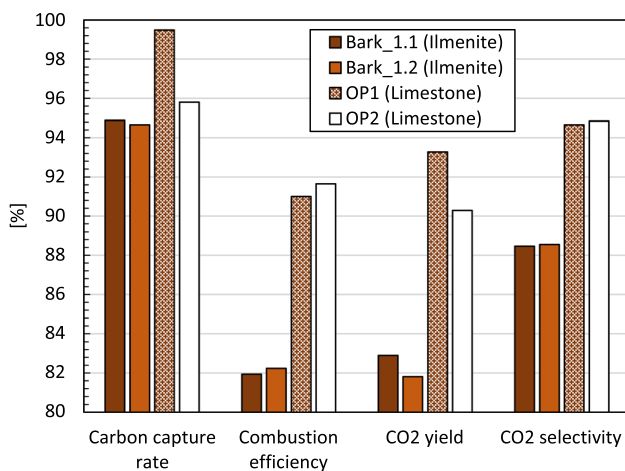
4.4 Exhaust gas treatment and coupled processes

The most proposed concept of post-gas treatment for CLC exhaust gas from the FR with solid fuels is the oxy-polishing process. The unconverted gas in the FR exhaust gas is combusted with pure O_2 in an additional reactor. Depending on conversion rates in the FR, more or less O_2 must be added. For optimal conditions in the oxy-polishing reactor, modelling predicts that it is possible to reach a percentage of unconverted gases and surplus oxygen of only 0.6%, which could be sufficient depending on the CO_2 storage application [64]. The downside of this process is the additional energy demand for oxygen separation from air, which is estimated to be over 0.3 kWh/kgO_2 for cryogenic separation [65]. For example, for a full combustion of OP1 and OP2 at least 1.8 and 1.3 kgO_2 per hour would have been necessary, which means an overall penalty to the process

Fig. 9 Performance parameter of the 80 kW$_{th}$ pilot plant in comparison pure ilmenite (Bark_1.1/1.2) and Ilmenite mixed with limestone (OP1/2)

efficiency between 0.6 to 0.8%, similar to values found in literature [60]. As an alternative to CO_2 storage, the direct methanation of the exhaust gas from the FR in a fluidized bed reactor is investigated during the experiments. About 5% exhaust gas of OP1 and OP2 was cleaned through a scrubber and activated carbon adsorbers. It was then methanated in a fluidized bed reactor at 360 °C and atmospheric pressure with additional hydrogen in the presence of a Ni catalyst. During OP2, the amount of hydrogen added to the exhaust gas was varied, resulting in a stoichiometric number (SN) of 1.29 (OP2a) and 1.17 (OP2b). The raw-SNG of the methanation reactor showed high concentrations of methane and unconverted hydrogen but very low CO_2 and CO concentrations during operation, as shown in Fig. 10. The excessive amount of hydrogen led to CO_2 and CO concentrations well below 1 vol.-%$_{db}$ and 0.1 vol.-%$_{db}$, respectively. OP2a, with the highest amount of hydrogen added, showed the highest conversion rates and yields except for the hydrogen conversion. X_{H2} was 7 percentage points lower at OP2a than during the other OPs, resulting in an unconverted hydrogen share of 25%. Further investigation of the methanation unit showed that it is possible to reach even lower CO concentrations with a higher amount of hydrogen [47] or a pressurized application of the methanation reactor. The concentration of CO and CO_2 would then be sufficiently low to be fed into the gas grid, although the excess hydrogen still needs to be separated and recycled.

For the purpose of comparing and evaluating the whole process chain of each experiment, the methanation unit was scaled up for processing the total amount of the fuel reactor exhaust gas. For converting the total FR exhaust gas amount, the methanation unit needed to handle around 30 times the initial gas input. As performance parameters, the carbon utilization and the CGE were calculated, see Table 5. OP1 showed the highest carbon utilization of 97%, resulting from the high carbon capture rate in the CLC plant. Lost carbon is a result of char transported to the AR, tars separated in the gas cleaning steps and unconverted carbon (CO and CO_2) in the methanation unit. The carbon utilization of

OP2a was close to the carbon capture rate of the CLC unit because of the high amount of excess H_2, whereby most of the carbon was converted to methane. Table 5 additionally shows a comparison of other fluidized bed technologies utilizing biogenic feedstock [66]. DFB steam gasification and sorption enhanced reforming combined with methanation show a lower carbon utilization but less amount of excessive hydrogen in the raw-SNG compared to CLC. Sorption enhanced reforming reaches the lowest value regarding carbon utilization because limestone is actively used to reduce the CO_2 and to increase H_2 concentrations in the product gas [67]. With no or less additional hydrogen needed, the CGE is, on the other hand, higher in the case of the gasification processes. The main advantages of the coupling of CLC with a methanation unit in comparison to the other processes are the higher heat generation during the process, the high carbon utilization rate and the low tar content in the FR exhaust gas, possibly omitting gas cleaning steps. However, high amounts of green hydrogen are needed.

Figure 11 depicts the mass flows of the different gases during OP2a with a scaled-up methanation unit. 13.7 kg/h bark pellets were combusted in the FR with 14.7 kg/h of O_2 released from the OC. The FR is fluidized with steam, which was then condensed and separated along with the tars from the FR exhaust gas in the biodiesel scrubber. Additional carbon loss resulted from the carbon slip between AR and FR in an amount of 260 g/h. The FR exhaust gas, mainly consisting of 20.3 kg/h CO_2, was transported to the fluidized bed methanation unit, where it is mixed with 4.4 kg/h of external hydrogen for the scaled-up methanation unit. With this amount of excess hydrogen and the reactive nickel catalyst, it is possible to decrease the mass flow of CO to 15 g/h. All in all, it would be possible to produce 7.5 kg/h of methane out of 13.7 kg of bark pellets. Depending on the natural gas grid feed-in specifications, it may be necessary to execute further gas upgrading. Mainly, a separation of the excessive hydrogen from the methane should be included to recycle hydrogen and decrease the external hydrogen demand of the methanation unit.

Fig. 10 Concentration and KPIs of the raw-SNG downstream the methanation unit (OP1 with oil addition and autothermal OP2b with lower surplus of hydrogen, autothermal OP2a with high surplus of hydrogen)
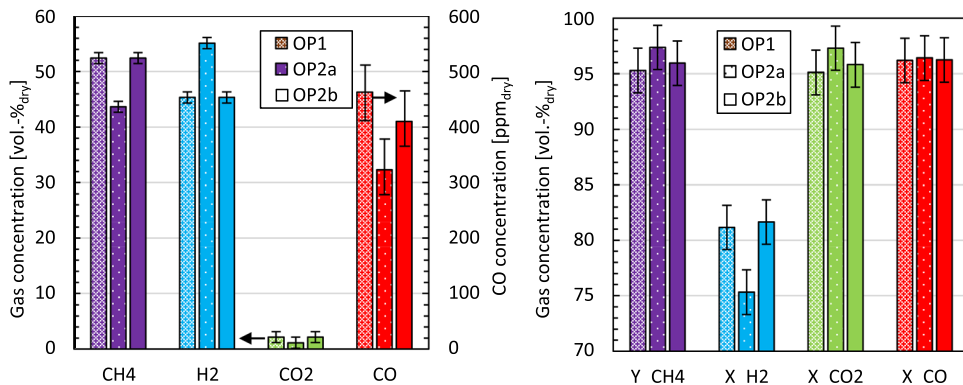
Table 5 Key performance indicators for SNG production via the CLC process chain in comparison to other DFB technologies

Process chain KPIs	Additional hydrogen added for methanation	Stoichiometric number	Carbon utilization	Cold gas efficiency
		[-]	[%]	[%]
OP1	Yes	1.17	97.0 ± 3.5	48.1 ± 3.5
OP2a	Yes	1.29	95.2 ± 3.7	47.4 ± 3.7
OP2b	Yes	1.17	93.8 ± 3.7	50.1 ± 3.7
Data from literature (Bartik et al. submitted manuscript: Experimental investigation of hydrogen-intensified synthetic natural gas production via biomass gasification: A technical comparison of different production pathways)				
DFB steam gasification	Yes	0.91	68.2	51.7
DFB steam gasification	No	0.30	37.3	53.1
DFB sorption enhanced reforming	No	0.71	35.6	62.4

Hydrogen, which must come from green sources, would be the main cost driver for the coupling of these technologies. For electrolysis, the production of 4.4 kg/h hydrogen of OP2a would have an energy demand of 211.15 kW [68], whereby no hydrogen recycle is included, which would decrease the amount of needed hydrogen. Another option of green hydrogen production is the chemical looping hydrogen (CLH) process, where biomass can be utilized to produce hydrogen with high purity. In CLH, a reduced OC splits steam by incorporating the oxygen [69–71]. In the context of this work, electrolysis was selected, because it opens up the interesting possibility to couple the process with CO_2 storage in addition to the methane production out of a CLC plant. Splitting the FR exhaust gas stream has the advantage of using mainly excess electricity for hydrogen production and therefore minimizing the costs for the hydrogen supply. Life cycle assessment showed a high potential for linking CLC with the methanation and the storage process [36]. A by-product of the hydrogen production via electrolysis is pure oxygen, which in this case could be used in the oxy-polishing step of the CO_2 storage route. In the following chapter, a scale-up of this concept based on the experimental results is discussed in combination with the electrolysis technology.
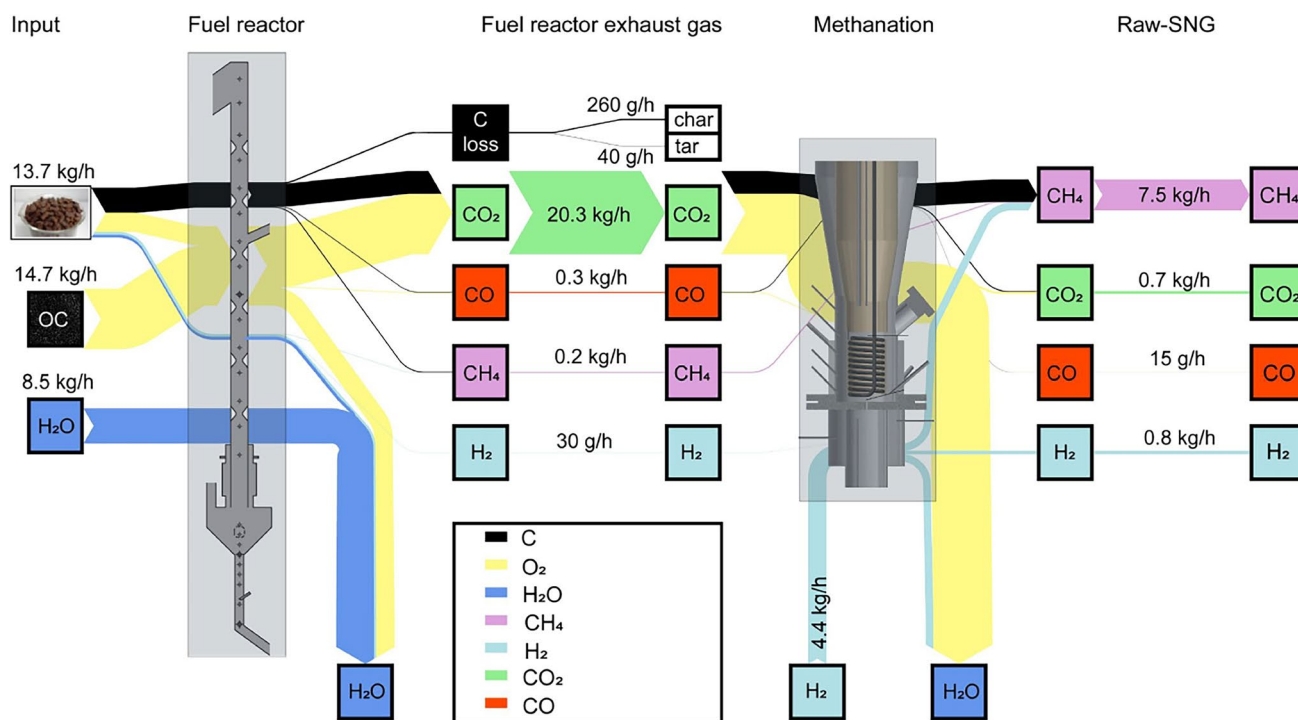
Fig. 11 Sankey diagram of the process chain of the 80 kWth pilot plant and scaled up fluidized bed methanation unit at TU Wien for OP2a

4.5 Scale-up simulation of a 100 MW$_{th}$ plant

Figure 12 (detailed in Figure S1 of the supplementary) shows the flow sheet of the simulated and upscaled experimental data of OP2a in the simulation software IPSEpro. The simulation is an extrapolation of the experimental results to higher fuel input. Efficiencies and heat loss are set according to industrial processes to calculate realistic mass and energy balance of OP2a with upscaled power in and output. As input, 100 MW$_{th}$ of bark pellets, compressed air, desalinated water for the water steam cycle and, depending on the calculation case, excess electricity for the proton exchange membrane (PEM) electrolysis are considered. Oxygen carrier makeup to compensate for attrition and dilution with ash is neglected in the simulation, but should be included in further studies to evaluate the ecological impact. The green CO_2 route starts with the fuel input to the FR, where 22 t/h of bark is converted by reaction with the oxygen of the ilmenite/limestone mixture to a gas with the composition of OP2a. The major part of the FR exhaust gas enters the oxy-polishing chamber and is mixed with pure oxygen from a pressure tank, which is supplied by a PEM electrolysis. After the heat recovery and a cleaning step, the CO_2 is pressurized and ready for gas storage. The reached quality of the CO_2 is also highly depending on the fuel input and its impurities. A detailed description of the necessary cleaning steps is given in literature [25]. The smaller part of the exhaust gas is directed to the methane route (shown in purple), where the exhaust gas is prepared for the methanation. Remaining amounts of tars and SO_X are removed in a scrubber and activated carbon adsorbers. The cleaned FR exhaust gas is mixed with hydrogen from the PEM electrolysis and directed to the fluidized bed methanation unit. The concentrations of the undesired components like CO and CO_2 are reduced by the hydrogen as demonstrated in OP2a. The hydrogen is separated via a polyimide membrane Matrimid 5218 [72] and recycled back to the methanation unit. The retentate with a low hydrogen concentration is already pressurized and after a further gas cleaning step ready for the gas grid. The AR exhaust gas (shown in red), with a low oxygen concentration, can be released to the atmosphere after the heat recovery. The generated heat in the CLC process is used for preheating the fluidization air and for steam production in a water-steam cycle. The water-steam cycle works at a pressure of 80 bar, uncoupling electricity via steam turbines and providing heat at 140 °C for district heating. The efficiency and additional data are given in Table S2 of the supplementary material.

The simulation was carried out for six different cases, see Table 6. The input power in every case is composed of fuel input of bark and the electricity needed for the PEM electrolysis, compressors and pumps. The power of the electrolysis determines the amount of produced H_2 and O_2, which are needed for the methanation and the oxy-polishing respectively. The output describes the produced shares of electricity by the turbine, generated methane and heat. The total efficiency is calculated by dividing output and input. The line "Net" provides information about the amount of stored CO_2, the O_2 balance and the electricity balance in the process, because O_2 and electricity is also consumed. In the first case (Case 1) the PEM electrolysis is supplied with enough energy

Fig. 12 Simplified flow chart of the simulation of 100 MW scale-up of the combination of the chemical looping combustion, methanation and electrolysis based on the experimental data of OP2a. The exact interconnections are given in Figure S1 of the supplementary material
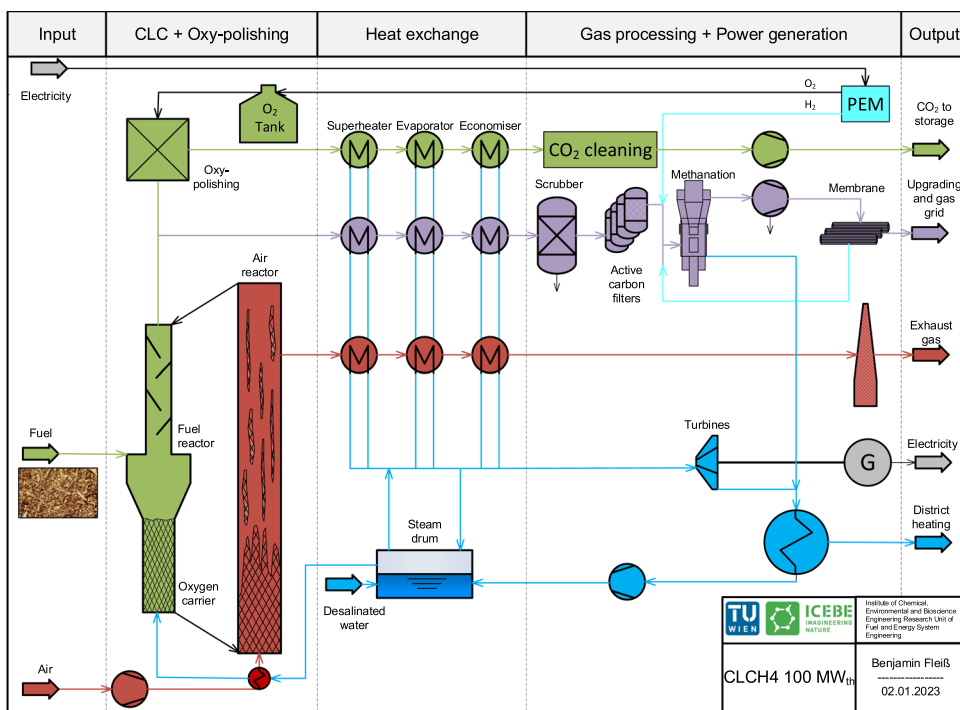
to produce sufficient oxygen for the oxy-polishing step. The electricity demand of the PEM electrolysis and the compressors for this case is low enough that the electricity produced by the turbines is sufficient and no further external electricity is needed. With the produced O_2 from the electrolysis, it is possible to generate 8.3 MW of methane. Case 2 and 3 cover high electricity prices, where the production and selling of electricity is more viable than that of methane. In Case 2, the amount of generated methane is reduced compared to Case 1 and 5 MW of electricity can be produce. Case 3 shows pure CO_2 storage and therefore no methane is produced. This case shows the highest total efficiency because of the omitting of the low efficiency of the electrolysis. For the gas treatment of the FR exhaust gas, up to 2.4 t/h of oxygen is needed for the oxy-polishing step, which can be discharged out of the O_2 tank or has to be externally supplied. In contrast, Case 4 and 5 describe the usage of renewable, external and surplus electricity to the extent of 10 and 100 MW. More oxygen is produced then used in the oxy-polishing step and the O_2 tank can be filled. Also, the compressor demand is increased due to higher volume flow to the membrane and the recirculation of hydrogen separated after the methanation unit. For a methanation of the total CO_2 stream, 291.2 MW of surplus electricity would be needed for power-to-methane (Case 6), where it is possible to produce 172.9 MW of methane. The high amount of green electricity and the low electric energy conversion efficiency in power-to-methane, including the annual number of operating hours and the thermal-to-electric conversion efficiency of methane make this case unfeasible for CLC, according to literature [35, 73].

The operation of a real plant should be located between case 3 and case 4 depending on electricity costs, availability of renewable external surplus electricity and filling state of the O_2 tank. This would also place the process in the field of the highest total efficiency. This requires a high operational flexibility of the PEM electrolysis and the methanation unit. PEM electrolysis cells are modular in their design and show short start-up times [68], which could benefit variable operation modes if the PEM electrolysis is oversized compared to the standard operation (Case 1) of the plant. As for fluidized beds, the methanation unit should have cost advantages for scale-up compared to fixed be reactors. In addition, fluidized beds can be designed to be designed to allow for a part load behaviour with regard to flexibility. This results in a plant that would be less sensitive to fluctuations in electricity and natural gas prices. The main output of the plant would be district heat and pure CO_2 for negative emissions. As for by-products, the share of electricity and methane can be balanced with the current price and can benefit the stabilisation of the electrical grid. Bareschino et al. [35] rate the environmental impact of the production and disposal of the OC as most critical in their life cycle assessment. Itis based on a synthetic CuO supported on zirconia as OC, which is a major difference to the natural ores that are used in this work. Navajas et al. report the lowest global warming potential of bio CLC with methanation and CO_2 storage compared to other power-to-gas processes to date, where three different OC are investigated [36].

5 Conclusion

In this work, a process chain experiment of an 80 kW$_{th}$ pilot plant for chemical looping combustion (CLC) with solid fuels combined with a fluidized bed methanation unit is presented. Bark pellets are converted with ilmenite as oxygen carrier enhanced by limestone to exhaust gas, which is methanated with hydrogen addition over a nickel catalyst. Operation conditions, gas compositions, conversions and yields of the individual and coupled processes were investigated.

Table 6 Simulation results of different calculation cases for 100 MW fuel input (Case 1: no additional electricity, Case 2: Producing 5 MW electricity, Case 3: CO_2 storage, Case 4: using 10 MW excess electricity, Case 5: using 100 MW excess electricity, Case 6: power-to-methane). The efficiency and additional data are given in Table S2 of the supplementary material

	Unit	Case 1	Case 2	Case 3	Case 4	Case 5	Case 6
Input							
Fuel input	MW	100.0	100.0	100.0	100.0	100.0	100.0
PEM electricity demand	MW	13.8	9.1	0.0	23.2	107.3	286.0
Compressors and O_2-tank demand	MW	8.1	7.8	7.2	8.7	14.3	26.1
Output							
Turbine electricity	MW	21.9	21.9	21.9	21.8	21.5	20.9
Generated district heating	MW	58.0	58.0	58.1	57.9	56.9	54.9
Exothermal heat methanation	MW	1.5	1.0	0	2.5	11.5	30.6
Generated methane	MW	8.3	5.5	0.0	14.0	64.9	172.9
Net							
CO_2 for storage	t/h	33.2	33.8	34.9	32.1	21.8	0.0
Net O_2 to tank	t/h	0.0	-0.8	-2.4	1.6	16.2	47.3
Net electricity	MW	0.0	5.0	14.8	-10.0	-100.0	-291.2
Total efficiency	%	73.6	73.9	74.7	72.9	69.9	67.3

Additionally, a scale-up concept for a 100 MW$_{th}$ plant based on the experimental results is proposed, combining the utilization and the storage of biogenic CO_2. The findings can be summarized as follows:

- High carbon capture rates and a combustion efficiency of over 91.7% were reached in the biomass CLC process, which was the best performance in the 80 kW$_{th}$ pilot plant with natural ores so far.
- During chemical looping combustion operation in the 80 kW$_{th}$ oil addition was used to increase the temperature and therefore the carbon capture rate. On the other hand, autothermal operation showed higher gas conversion due to higher oxygen uptake in the air reactor.
- The addition of limestone to ilmenite increased all key performance indicators in comparison to a former experimental campaign with pure ilmenite by 5–10%. Through higher conversion rates, the temperature was increased, which again favored the conversion and carbon capture.
- The pilot plant was successfully coupled with a fluidized bed methanation unit and almost all input was converted with external hydrogen addition to methane, reaching a methane yield of over 97%.
- The process chain experiment showed higher carbon utilization (95.2%) but lower cold gas efficiency (47.4%) compared to other dual fluidized bed gasification technologies coupled with methanation.
- The scale-up simulation of the experimental data to a 100 MW$_{th}$ plant, combining the CO_2 methanation with storage, revealed a high potential with regard to adaptability, global warming potential reduction and promising high total efficiencies between 65 and 75%.

Based on these findings, a techno-economic analysis and life cycle assessment of the scaled-up results could provide information on the competitiveness compared to other technologies in the field of renewable energy generation, CO_2 storage and power-to-gas.

Abbreviations *AR*: Air reactor; *BECCS*: Bioenergy with Carbon Capture & Storage; *CGE*: Cold gas efficiency; *CLC*: Chemical looping combustion; *CLH*: Chemical looping hydrogen; *CLOU*: Chemical looping with oxygen uncoupling; C_nH_m: Fuel; *DFB*: Dual fluidized bed; *FR*: Fuel reactor; *ILS*: Inner loop seal; *KPI*: Key performance indicator; *LLS*: Lower loop seal; MeO_x: Metal oxide; *OC*: Oxygen carrier, oxygen carriers; *OP*: Operating point; *PEM*: Proton exchange membrane; *SCR*: Solid circulation rate; *SNG*: Synthetic natural gas; *ULS*: Upper loop seal; *UV*: Ultraviolet; $\dot{n}_{C,FR,exhaust}[mol/s]$: Mol flow of carbon FR exhaust; $\dot{n}_{C,CH_4,out}[mol/s]$: Mol flow of carbon of methane in raw SNG after methanation; $\dot{n}_{CO2,FR,exhaust}[mol/s]$: Mol flow of carbon dioxide FR exhaust; $\dot{n}_{C,FR,feed}[mol/s]$: Mol flow of carbon FR fuel feed; $\dot{n}_{O_2,fuel,dem}[mol/s]$: Mol flow of oxygen for combustion FR fuel feed; $\dot{n}_{O_2,exhaust,dem}[mol/s]$: Mol flow of oxygen for combustion FR exhaust; $\dot{n}_{i,feed}[mol/s]$: Mol flow of gas i to the methanation unit; $\dot{n}_{i,out}[mol/s]$: Mol flow of gas i after the methanation unit; $N_i[-]$: Number of carbons of component i; $P_{CH4},out[kW]$: Chemical energy of methane in SNG; $P_{fuel},FR[kWth]$: Fuel power input of the fuel reactor; $P_{H2}[kW]$: Chemical energy of hydrogen input; $P_{oil}[kWth]$: Oil power input to the air reactor; $S/C[-]$: Steam to carbon ratio; $S_{CO2}[\%]$: Selectivity of gas specie CO_2; $SCR[kg/h]$: Solid circulation rate between air and fuel reactor; $S_n[\%]$: Selectivity of certain gas specie; $SN[-]$: Stoichiometric number of hydrogens in methanation unit; $X_C[\%]$: Carbon conversion; $X_{SNG,i}[\%]$: Conversion of component i in the methanation unit; Y_{CO2}: [%]Yield of CO2; $y_i[-]$: Molar fraction of component i; $Y_n[\%]$: Yield of certain gas specie; $Y_{SNG},CH4[\%]$: Yield of CH4 in the methanation unit; $\Delta H_R^0[kJ/mol]$: Reaction enthalpy; $\eta_C,total[\%]$: Carbon utilization of whole chain; $\eta_{CC}[\%]$: Carbon capture rate CLC pilot plant; $\eta_{comb}[\%]$: Combustion efficiency; $\vartheta AR_{exh}[°C]$: Temperature of air reactor exhaust gas; $\vartheta FR_{exh}[°C]$: Temperature of fuel reactor exhaust gas; $\vartheta FR_{low}[°C]$: Temperature of lower fuel reactor; $\lambda[-]$: Air to fuel ratio; $\varphi[kg/kg]$: Oxygen of OC to fuel ration; $\Omega_{OD}[\%]$: Oxygen demand for full combustion

Author contributions All persons who meet authorship criteria are listed as authors, and all authors certify that they have participated sufficiently in the work to take public responsibility for the content, including participation in the concept, design, analysis, writing, or revision of the manuscript. Category 1: Conception and design of study: Fleiß B., Benedikt F., Fuchs J., Hofbauer H.; acquisition of data: Fleiß B., Priscak J., Bartik A.; analysis and/or interpretation of Fleiß B., Fuchs J., Priscak J., Müller S. Category 2: Drafting the manuscript: Fleiß B., Fuchs J.; revising the manuscript critically for important intellectual content: Bartik A., Priscak J., Benedikt F., Fuchs J., Müller S., Hofbauer H. Category 3: Approval of the version of the manuscript to be published (the names of all authors must be listed): Fleiß B., Bartik A., Priscak J., Benedikt F., Fuchs J., Müller S., Hofbauer H.

Data availability Data will be made available on request.

Declarations

Ethical approval Not applicable.

Competing interests The authors declare that they have no known competing financial interests or personal relationships that could have appeared to influence the work reported in this paper.

References

1. Penthor S, Fuchs J, Benedikt F, Schmid J, Mauerhofer A, Mayer K, Hofbauer H (2018) First results from an 80 kW dual fluidized bed pilot unit for solid fuels at TU Wien, in 5th International Conference on Chemical Looping. Park City, Utah, USA

2. Benedikt F, Kuba M, Schmid JC, Müller S, Hofbauer H (2019) Assessment of correlations between tar and product gas composition in dual fluidized bed steam gasification for online tar prediction. Appl Energy 238:1138–1149. https://doi.org/10.1016/j.apenergy.2019.01.181

3. Fleiß B, Penthor S, Müller S, Hofbauer H, Fuchs J (2022) Holistic assessment of oxygen carriers for chemical looping combustion based on laboratory experiments and validation in 80 kW pilot plant. Fuel Process Technol. 231 https://doi.org/10.1016/j.fuproc.2022.107249

4. Czakiert T, Krzywanski J, Zylka A, Nowak W (2022) Chemical Looping Combustion: A Brief Overview. Energies. 15(4) https://doi.org/10.3390/en15041563

5. Adánez J, Abad A, Mendiara T, Gayán P, de Diego LF, García-Labiano F (2018) Chemical looping combustion of solid fuels. Prog Energy Combust Sci 65:6–66. https://doi.org/10.1016/j.pecs.2017.07.005

6. Di Giuliano A, Capone S, Anatone M, Gallucci K (2022) Chemical Looping Combustion and Gasification: A Review and a Focus on European Research Projects. Ind Eng Chem Res 61(39):14403–14432. https://doi.org/10.1021/acs.iecr.2c02677

7. Solomon S, Qin D, Manning M, Chen Z, Marquis M, Averyt KB, Tignor M, Miller HL (2007) Climate Change 2007: The Physical Science Basis. Contribution of Working Group I to the Fourth Assessment Report of the Intergovernmental Panel on Climate Change. IPCC. 4

8. Rydén M, Lyngfelt A, Langørgen Ø, Larring Y, Brink A, Teir S, Havåg H, Karmhagen P (2017) Negative CO2 Emissions with Chemical-Looping Combustion of Biomass – A Nordic Energy Research Flagship Project. Energy Procedia 114:6074–6082. https://doi.org/10.1016/j.egypro.2017.03.1744

9. Sun Y, Dong B, Wang L, Li H, Thorin E (2022) Technology selection for capturing CO2 from wood pyrolysis. Energy Convers \Manag.266 . https://doi.org/10.1016/j.enconman.2022.115835

10. Mercado JP, Ubando AT, Gonzaga JA, Naqvi SR (2023) Life cycle assessment of a biomass based chemical looping combustion. Environ Res 217:114876. https://doi.org/10.1016/j.envres.2022.114876

11. Gizer SG, Polat O, Ram MK, Sahiner N (2022) Recent developments in CO2 capture, utilization, related materials, and challenges. Int J Energy Res 46(12):16241–16263. https://doi.org/10.1002/er.8347

12. Pröll T, Lyngfelt A (2022) Steam Methane Reforming with Chemical-Looping Combustion: Scaling of Fluidized-Bed-Heated Reformer Tubes. Energy Fuels 36(17):9502–9512. https://doi.org/10.1021/acs.energyfuels.2c01086

13. Abad A, Gayán P, García-Labiano F, de Diego LF, Izquierdo MT, Mendiara T, Adánez J (2022) Relevance of oxygen carrier properties on the design of a chemical looping combustion unit with gaseous fuels. Greenhouse Gases: Sci Technol https://doi.org/10.1002/ghg.2170

14. Lyngfelt A, Brink A, Langørgen Ø, Mattisson T, Rydén M, Linderholm C (2019) 11,000 h of chemical-looping combustion operation—Where are we and where do we want to go? Int J Greenhouse Gas Control 88:38–56. https://doi.org/10.1016/j.ijggc.2019.05.023

15. Filsouf A, Adánez-Rubio I, Mendiara T, Abad A, Adánez J (2023) Developing magnetic, durable, agglomeration resistant and reactive copper-based oxygen carrier particles by promoting a kaolin-reinforced, manganese-iron mixed oxide support. Fuel Process Technol. 241 https://doi.org/10.1016/j.fuproc.2022.107616

16. Liu G, Lisak G (2023) Cu-based oxygen carriers for chemical looping processes: Opportunities and challenges. Fuel. 342 https://doi.org/10.1016/j.fuel.2023.127828

17. Li L, Wang Y, Bu H, Xu Z, Zhao H (2022) Semi-continuous Operation of Chemical Looping Combustion of Coal Using a Low-Cost Composite Oxygen Carrier. Energy Fuels 36(17):9450–9459. https://doi.org/10.1021/acs.energyfuels.2c01153

18. Barros do Nascimento RA, Pimenta de Macedo H, Melo DMA, Santiago RC, Rodrigues de Araújo T, Medeiros RLBA, Adánez J (2022) Structure and Reactivity of Brazilian Iron Ores as Low-Cost Oxygen Carriers for Chemical Looping Combustion. Industr Eng Chem Res. 61(6): 2469-2482 https://doi.org/10.1021/acs.iecr.1c03763

19. Di Z, Yilmaz D, Biswas A, Cheng F, Leion H (2022) Spinel ferrite-contained industrial materials as oxygen carriers in chemical looping combustion. Applied Energy. 307 https://doi.org/10.1016/j.apenergy.2021.118298

20. Linderholm C, Lyngfelt A, Dueso C (2013) Chemical-looping combustion of solid fuels in a 10kW reactor system using natural minerals as oxygen carrier. Energy Procedia 37:598–607. https://doi.org/10.1016/j.egypro.2013.05.147

21. Gu H, Shen L, Zhong Z, Niu X, Liu W, Ge H, Jiang S, Wang L (2015) Cement/CaO-modified iron ore as oxygen carrier for chemical looping combustion of coal. Appl Energy 157:314–322. https://doi.org/10.1016/j.apenergy.2015.06.023

22. Lyngfelt A (2020) Chemical Looping Combustion: Status and Development Challenges. Energy Fuels 34(8):9077–9093. https://doi.org/10.1021/acs.energyfuels.0c01454

23. Lin J, Luo K, Hu C, Sun L, Fan J (2022) Full-loop simulation of a 1 MWth pilot-scale chemical looping combustion system. Chemical Engineering Science. 249 https://doi.org/10.1016/j.ces.2021.117301

24. Gogolev I, Linderholm C, Gall D, Schmitz M, Mattisson T, Pettersson JBC, Lyngfelt A (2019) Chemical-looping combustion in a 100 kW unit using a mixture of synthetic and natural oxygen carriers – Operational results and fate of biomass fuel alkali. Int J Greenhouse Gas Control 88:371–382. https://doi.org/10.1016/j.ijggc.2019.06.020

25. Lyngfelt A, Petersson L, Andersson K (2022) Downstream Gas Treatment to Attain Storage Quality of CO2 from Chemical-Looping Combustion. in 6th International Conference on Chemical Looping. Zaragoza, Spain

26. Lindmüller L, Haus J, Ramesh Kumar Nair A, Heinrich S (2022) Minimizing gas leakages in a system of coupled fluidized bed reactors for chemical looping combustion. Chem Eng Sci. 250 https://doi.org/10.1016/j.ces.2021.117366

27. Zhang Q, Cao Z, Ye S, Sha Y, Chen B, Zhou H (2022) Mathematical modeling for bubbling fluidized bed CO-methanation reactor incorporating the effect of circulation and particle flows. Chem Eng Sci. 249 https://doi.org/10.1016/j.ces.2021.117305

28. Coppola A, Massa F, Scala F (2023) Simulation of a sorption-enhanced methanation process with CaO in a dual interconnected fluidized bed system. Fuel. 339 https://doi.org/10.1016/j.fuel.2022.127374

29. Yamamoto S, Sayama S, Kunitomi S, Ogasawara K, Baba N (2022) Demonstration of a high-efficiency carbon dioxide capture and methanation system with heat/material integration for power-to-gas and zero carbon dioxide emissions in flue gasses. Int J Greenhouse Gas Control. 114 https://doi.org/10.1016/j.ijggc.2022.103584

30. Wen D, Aziz M (2022) Design and analysis of biomass-to-ammonia-to-power as an energy storage method in a renewable multi-generation system. Energy Convers Manag. 261 https://doi.org/10.1016/j.enconman.2022.115611

31. Surywanshi GD, Pillai BBK, Patnaikuni VS, Vooradi R, Anne SB (2019), Formic acid synthesis – a case study of CO2 utilization from coal direct chemical looping combustion power plant. Energy Sources, Part A: Recover Utilization Environ Effects. 44(1): 2220–2235 https://doi.org/10.1080/15567036.2019.1649325

32. He Y, Zhu L, Fan J, Li L, Liu G (2021) Life cycle assessment of CO2 emission reduction potential of carbon capture and utilization for liquid fuel and power cogeneration. Fuel Process Technol. 221 https://doi.org/10.1016/j.fuproc.2021.106924

33. Piroozmand M, Hafizi A (2022) Assessment of a novel coupling integrated process for coproducing syngas and hydrogen from natural gas and biomass feedstocks with in-situ CO2 utilization. Energy Convers Manag. 254 https://doi.org/10.1016/j.enconman.2022.115241

34. Bareschino P, Mancusi E, Urciuolo M, Coppola A, Solimene R, Pepe F, Chirone R, Salatino P (2020) Modelling of a combined biomass CLC combustion and renewable-energy-based methane production system for CO2 utilization. Powder Technol 373:421–432. https://doi.org/10.1016/j.powtec.2020.06.059

35. Bareschino P, Mancusi E, Urciuolo M, Paulillo A, Chirone R, Pepe F (2020) Life cycle assessment and feasibility analysis of a combined chemical looping combustion and power-to-methane system for CO2 capture and utilization. Renew Sustain Energy Rev. 130 https://doi.org/10.1016/j.rser.2020.109962

36. Navajas A, Mendiara T, Gandía LM, Abad A, García-Labiano F, de Diego LF (2022) Life cycle assessment of power-to-methane systems with CO2 supplied by the chemical looping combustion of biomass. Energy Convers Manag. 267 https://doi.org/10.1016/j.enconman.2022.115866

37. Brachi P, Bareschino P, Tregambi C, Pepe F, Urciuolo M, Ruoppolo G, Mancusi E (2023) Assessing the feasibility of an integrated CLC-methanation system using solar dried and torrefied biomasses as a feedstock. Fuel. 331 https://doi.org/10.1016/j.fuel.2022.125951

38. Adánez J, Abad A (2019) Chemical-looping combustion: Status and research needs. Proc Combust Inst 37(4):4303–4317. https://doi.org/10.1016/j.proci.2018.09.002

39. Coppola A, Scala F (2021) Chemical Looping for Combustion of Solid Biomass: A Review. Energy Fuels 35(23):19248–19265. https://doi.org/10.1021/acs.energyfuels.1c02600

40. Idziak K, Czakiert T, Krzywanski J, Zylka A, Kozlowska M, Nowak W (2020) Safety and environmental reasons for the use of Ni-, Co-, Cu-, Mn- and Fe-based oxygen carriers in CLC/CLOU applications: An overview. Fuel. 268 https://doi.org/10.1016/j.fuel.2020.117245

41. Adánez-Rubio I, Bautista H, Izquierdo MT, Gayán P, Abad A, Adánez J (2021) Development of a magnetic Cu-based oxygen carrier for the chemical looping with oxygen uncoupling (CLOU) process. Fuel Process Technol. 218 https://doi.org/10.1016/j.fuproc.2021.106836

42. Bartik A, Fuchs J, Müller S, Hofbauer H (2020) Development of an internally circulating fluidized bed for catalytic methanation of syngas, in Proceedings of the 16th Minisymposium Verfahrenstechnik and 7th Partikelforum. Vienna

43. Pröll T, Hofbauer H (2010) A dual fluidized bed system for chemical looping combustion of solid fuels. Proceedings of the AIChE Annual Meeting 2010 Salt Lake City, USA

44. Schmid J, Pröll T, Pfeifer C, Hofbauer H (2011) Improvement of gas-solid interaction in dual circulating fluidized bed systems, in Proceedings of the 9th Conference on Industrial Furnances and Boilers (INFUB-9) Estoril, Portugal

45. Lunzer A, Kraft S, Müller S, Hofbauer H (2021) CPFD simulation of a dual fluidized bed cold flow model. Biomass Convers Bioref 11(1):189–203. https://doi.org/10.1007/s13399-020-01229-4

46. Fleiß B, Priscak J, Fuchs J, Müller S, Hofbauer H (2023) Synthetic oxygen carrier C28 compared to natural ores for chemical looping combustion with solid fuels in 80 kWth pilot plant experiments. Fuel. 334 https://doi.org/10.1016/j.fuel.2022.126816

47. Bartik A, Fuchs J, Pacholik G, Föttinger K, Hofbauer H, Müller S, Benedikt F (2022) Experimental Investigation on the Methanation of Hydrogen-Rich Syngas in a Bubbling Fluidized Bed Reactor Utilizing an Optimized Catalyst. Fuel Process Technol. FUPROC-D-22–00721 https://doi.org/10.2139/ssrn.4110983

48. Abad A, Adánez J, Cuadrat A, García-Labiano F, Gayán P, de Diego LF (2011) Kinetics of redox reactions of ilmenite for chemical-looping combustion. Chem Eng Sci 66(4):689–702. https://doi.org/10.1016/j.ces.2010.11.010

49. Adánez J, Cuadrat A, Abad A, Gayán P, de Diego LF, García-Labiano F (2010) Ilmenite Activation during Consecutive Redox Cycles in Chemical-Looping Combustion. Energy Fuels 24(2):1402–1413. https://doi.org/10.1021/ef900856d

50. Cuadrat A, Abad A, Adánez J, de Diego LF, García-Labiano F, Gayán P (2012) Behavior of ilmenite as oxygen carrier in chemical-looping combustion. Fuel Process Technol 94(1):101–112. https://doi.org/10.1016/j.fuproc.2011.10.020

51. Linderholm C, Schmitz M, Knutsson P, Lyngfelt A (2016) Chemical-looping combustion in a 100-kW unit using a mixture of ilmenite and manganese ore as oxygen carrier. Fuel 166:533–542. https://doi.org/10.1016/j.fuel.2015.11.015

52. Teyssié G, Leion H, Schwebel GL, Lyngfelt A, Mattisson T (2011) Influence of Lime Addition to Ilmenite in Chemical-Looping Combustion (CLC) with Solid Fuels. Energy Fuels 25(8):3843–3853. https://doi.org/10.1021/ef200623h

53. Mayer K (2010) Ilmenite and mixtures with Olivine as oxygen carriers in a chemical looping combustion pilot plant, in Fakultät für Technische Chemie | Institut für Verfahrenstechnik, Umwelttechnik und Technische Biowissenschaften, TU Wien: Wien

54. Fan JM, Hong H, Jin HG (2019) Life cycle global warming impact of CO2 capture by in-situ gasification chemical looping combustion using ilmenite oxygen carriers. J Clean Prod 234:568–578. https://doi.org/10.1016/j.jclepro.2019.06.082

55. Mauerhofer AM, Benedikt F, Schmid JC, Fuchs J, Müller S, Hofbauer H (2018) Influence of different bed material mixtures on dual fluidized bed steam gasification. Energy 157:957–968. https://doi.org/10.1016/j.energy.2018.05.158

56. Cuadrat A, Linderholm C, Abad A, Lyngfelt A, Adánez J (2011) Influence of Limestone Addition in a 10 kWth Chemical-Looping Combustion Unit Operated with Petcoke. Energy Fuels 25(10):4818–4828. https://doi.org/10.1021/ef200806q

57. Fleiß B, Fuchs J, Penthor S, Arlt S, Pachler R, Müller S, Hofbauer H (2021) Innovative laboratory unit for pre-testing of oxygen carriers for chemical-looping combustion. Biomass Convers Bioref. https://doi.org/10.1007/s13399-021-01530-w

58. Fleiß B, Priscak J, Fuchs J, Müller S, Hofbauer H (2023) Synthetic oxygen carrier C28 compared to natural ores for chemical looping combustion with solid fuels in 80 kWth pilot plant experiments. Fuel

59. Marx K, Bertsch O, Pröll T, Hofbauer H (2013) Next Scale Chemical Looping Combustion: process Integration and Part Load Investigations for a 10MW Demonstration Unit. Energy Procedia 37:635–644. https://doi.org/10.1016/j.egypro.2013.05.151

60. Lyngfelt A, Leckner B (2015) A 1000 MWth boiler for chemical-looping combustion of solid fuels – Discussion of design and costs. Appl Energy 157:475–487. https://doi.org/10.1016/j.apenergy.2015.04.057

61. Linderholm C, Schmitz M, Knutsson P, Källén M, Lyngfelt A (2014) Use of Low-Volatile Solid Fuels in a 100 kW Chemical-Looping Combustor. Energy Fuels 28(9):5942–5952. https://doi.org/10.1021/ef501067b

62. Schmid JC, Benedikt F, Fuchs J, Mauerhofer AM, Müller S, Hofbauer H (2019) Syngas for biorefineries from thermochemical gasification of lignocellulosic fuels and residues—5 years' experience with an advanced dual fluidized bed gasifier design. Biomass Convers Bioref. https://doi.org/10.1007/s13399-019-00486-2

63. Gogolev I, Soleimanisalim AH, Linderholm C, Lyngfelt A (2021) Commissioning, performance benchmarking, and investigation of alkali emissions in a 10 kWth solid fuel chemical looping combustion pilot. Fuel. 287 https://doi.org/10.1016/j.fuel.2020.119530

64. Mei D, Linderholm C, Lyngfelt A (2021) Performance of an oxy-polishing step in the 100 kWth chemical looping combustion prototype. Chem Eng J. 409 https://doi.org/10.1016/j.cej.2020.128202

65. Variny M, Jedina D, Rimar M, Kizek J, Ksinanova M (2021) Cutting Oxygen Production-Related Greenhouse Gas Emissions by Improved Compression Heat Management in a Cryogenic Air Separation Unit. Int J Environ Res Public Health. 18(19) https://doi.org/10.3390/ijerph181910370

66. Müller S, Theiss L, Fleiß B, Hammerschmid M, Fuchs J, Penthor S, Rosenfeld DC, Lehner M, Hofbauer H (2020) Dual fluidized bed based technologies for carbon dioxide reduction — example hot metal production. Biomass Convers Bioref 11(1):159–168. https://doi.org/10.1007/s13399-020-01021-4

67. Fuchs J, Schmid JC, Müller S, Hofbauer H (2019) Dual fluidized bed gasification of biomass with selective carbon dioxide removal and limestone as bed material: A review. Renew Sustain Energy Rev 107:212–231. https://doi.org/10.1016/j.rser.2019.03.013

68. Böhm H, Zauner A, Rosenfeld DC, Tichler R (2020) Projecting cost development for future large-scale power-to-gas implementations by scaling effects. Applied Energy. 264 https://doi.org/10.1016/j.apenergy.2020.114780

69. Luo M, Yi Y, Wang S, Wang Z, Du M, Pan J, Wang Q (2018) Review of hydrogen production using chemical-looping technology. Renew Sustain Energy Rev 81:3186–3214. https://doi.org/10.1016/j.rser.2017.07.007

70. Turap Y, Wang Z, Wang Y, Zhang Z, Chen S, Wang W (2023) High purity hydrogen production via coupling CO2 reforming of biomass-derived gas and chemical looping water splitting. Applied Energy. 331 https://doi.org/10.1016/j.apenergy.2022.120447

71. Bock S, Stoppacher B, Malli K, Lammer M, Hacker V (2021) Techno-economic analysis of fixed-bed chemical looping for decentralized, fuel-cell-grade hydrogen production coupled with a 3 MWth biogas digester. Energy Convers Manag. 250 https://doi.org/10.1016/j.enconman.2021.114801

72. Shalygin MG, Abramov SM, Netrusov AI, Teplyakov VV (2015) Membrane recovery of hydrogen from gaseous mixtures of biogenic and technogenic origin. Int J Hydrogen Energy 40(8):3438–3451. https://doi.org/10.1016/j.ijhydene.2014.12.078

73. Fózer D, Volanti M, Passarini F, Varbanov PS, Klemeš JJ, Mizsey P (2020) Bioenergy with carbon emissions capture and utilisation towards GHG neutrality: Power-to-Gas storage via hydrothermal gasification. Applied Energy. 280 https://doi.org/10.1016/j.apenergy.2020.115923